RESEARCH ARTICLE

Transition-Metal Doping and Biaxial Strain Tune Magnetism and Electronic Structure in Two-Dimensional GaN: A First-Principles Study

Yi Luo[1,*], **Weiye He**[1], **Jilin Xu**[1], **Lijie Zuo**[1], **Feng Shang**[1], **Wen Feng**[1] **and Qianyi Ma**[2]

[1] School of Mechanical Engineering, Jiangsu Ocean University, Lianyungang 222000, China
[2] Department of Chemical Engineering, University of Waterloo, Waterloo, ON N2L 3G1, Canada

Abstract

Pristine two-dimensional (2D) GaN is non-magnetic, which limits its direct use in semiconductor spintronics. Here, first-principles calculations were used to screen 3d transition-metal substitution (TM = Sc-Zn) at 6.25 at.% and 9.375 at.% and to evaluate biaxial strain from -3% to 3%. Co substitution produced the most favorable magnetic semiconductor response among the screened dopants. The two concentrations yielded magnetic moments of 8.00 and 12.00 μ_B per supercell and band gaps of 0.80 and 0.55 eV, respectively. Biaxial strain preserved the magnetic order while tuning the band gaps. In the 6.25 at.% Co-doped system, the gap reached 0.89 eV at 2% tensile strain and became direct at 3% tensile strain. These calculations identify Co substitution and moderate biaxial strain as a promising theoretical route for tuning the magnetic and electronic properties of monolayer GaN.

Keywords: two-dimensional GaN, transition-metal doping, biaxial strain, semiconductor spintronic devices, first-principles calculations.

1 Introduction

Semiconductor spintronics uses the spin degree of freedom, in addition to charge, for information storage and processing. Representative device concepts include magnetoresistive random-access memory [1, 2], spin logic devices [3, 4], spin transistors [5], and spin computation accelerators and multifunctional spintronic devices [6, 7]. Realizing these technologies requires semiconductors that combine controllable magnetism with suitable electronic and integration characteristics [8–10].

Two-dimensional (2D) materials provide a promising materials space for this purpose. Since the discovery of graphene, many 2D systems have been investigated, including transition-metal dichalcogenides [11], MXenes [12, 13], and hexagonal boron nitride [14]. Their atomic thickness, large surface-to-volume ratio, quantum-confinement effects, and mechanical flexibility have enabled applications in electronics [16, 17], energy conversion

Submitted: 28 June 2026
Revised: 09 August 2026
Accepted: 11 August 2026
Published: 17 August 2026

Vol. 2, **No.** 3, 2026.
10.62762/JAMR.2026.353789

***Corresponding author:**
✉ Yi Luo
yiluo9451@outlook.com

Citation
Luo, Y., He, W., Xu, J., Zuo, L., Shang, F., Feng, W., & Ma, Q. (2026). Transition-Metal Doping and Biaxial Strain Tune Magnetism and Electronic Structure in Two-Dimensional GaN: A First-Principles Study. *Journal of Advanced Materials Research*, 2(3), 236–250.

and storage [15, 18], flexible devices [19], optics [20], catalysis and environmental technologies [21], and neuromorphic computing [22]. These characteristics make 2D materials attractive candidates for overcoming scaling and functionality limitations in semiconductor spintronic devices.

GaN is already a key semiconductor for power electronics and optoelectronics because of its high power density, high-frequency response, and mature device ecosystem [24]. In 2016, Al Balushi et al. [25] realized single-atom-layer 2D GaN on graphene-encapsulated SiC by migration-enhanced encapsulated growth. The resulting 2D GaN can be viewed as an atomically thin analogue of three-dimensional GaN and has been predicted to exhibit high carrier mobility, a tunable band gap, and good thermal and chemical stability [26–28]. It can also be stabilized with retention of its fundamental electronic and magnetic properties upon various chemical modifications [29, 30]. However, pristine 2D GaN is non-magnetic [31], which limits its direct use in spintronic devices. A practical design strategy must therefore introduce magnetism while retaining a useful semiconductor band gap.

Chemical doping and biaxial strain are two widely used routes for modulating electronic structure and magnetic properties across a broad range of functional materials, including low-dimensional systems [23, 32–35]. For monolayer GaN, alkali-metal doping has been shown to produce magnetic semiconducting behavior, whereas alkaline-earth-metal doping can drive semimetallic behavior [36]. Related first-principles studies have also shown that V, Cr, and Mn substitution can induce magnetism in 2D Ga_2O_3 [37], and that strain can tune the band gap of doped 2D oxides. In ZnO, compositional tuning with nonmetal dopants has likewise been shown to modify the structural and optical properties [38]. These studies suggest that dopant selection and lattice strain can be combined to design magnetic semiconducting behavior, but the systematic response of transition-metal-doped 2D GaN across dopant concentration and strain remains insufficiently resolved.

Although prior first-principles studies have examined specific transition-metal dopants in GaN monolayers [47], a systematic comparison across the full 3d series at multiple concentrations combined with strain analysis has not been reported. To address this gap, this work investigates 3d transition-metal substitution (TM = Sc-Zn) in 2D GaN at 6.25 at.% and 9.375 at.% using first-principles calculations. The analysis focuses on structural stability, magnetic-moment formation, electronic band character, and the response of the most suitable doped systems to biaxial strain from -3% to 3%. The objective is to identify doped 2D GaN systems that combine stable magnetic ordering with a semiconductor band gap larger than 0.50 eV and to determine whether biaxial strain can tune that gap without destroying the desired magnetic semiconductor state.

2 Calculation Methods

First-principles calculations were performed using the Vienna Ab initio Simulation Package [39]. The projector augmented-wave method [40] and the Perdew-Burke-Ernzerhof generalized-gradient approximation [41] were used. Spin polarization was included in all doped-system calculations. The plane-wave cutoff energy was set to 550 eV, and a 20 Å vacuum layer was introduced perpendicular to the 2D GaN sheet to minimize spurious interactions between periodic images. No empirical van der Waals correction was included because the present systems are isolated monolayers rather than layered stacks or adsorption complexes. Brillouin-zone integrations were performed using a $9 \times 9 \times 1$ Γ-centered k-point grid. The total-energy and force convergence criteria were 10^{-6} eV and 10^{-2} eV Å^{-1}, respectively.

3 Results and Discussion

Pristine 2D GaN was first optimized to establish a reference structure. The relaxed monolayer adopts a planar hexagonal honeycomb structure, as shown in Figure 1 (a). The primitive unit cell contains one Ga atom and one N atom, and the optimized lattice constant is $a = b = 3.26$ Å. This value agrees well with previous density-functional-theory results of $a = b = 3.255$ Å [42, 43]. The corresponding Ga-N bond length is 1.88 Å. After relaxation of a $4 \times 4 \times 1$ supercell, the calculated band structure shows semiconducting behavior with an indirect band gap of 1.94 eV. The conduction-band minimum lies at Γ, whereas the valence-band maximum lies at K (Figure 1 (b)).

Transition-metal substitution was then introduced into the 2D GaN supercell at 6.25 at.% and 9.375 at.%. The corresponding structural models are shown in Figures 1 (c) and (d). For each doped structure, the TM-N bond length, dopant-vacancy binding energy, total magnetic moment, local magnetic moment on the dopant atom, and band gap were calculated to evaluate

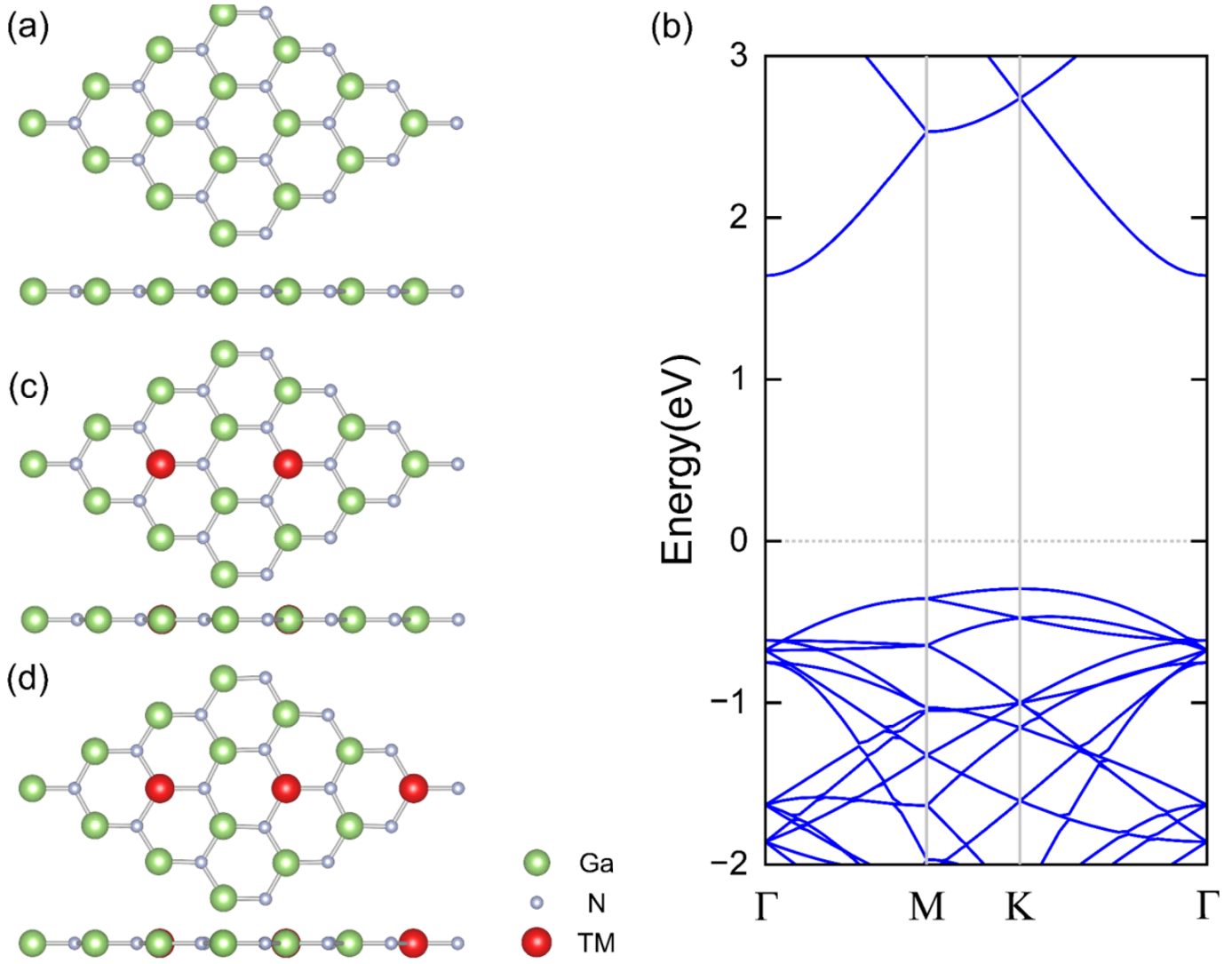

Figure 1. (a) Optimized pristine 2D GaN reference structure represented by a 4 × 4 × 1 supercell; (b) band structure of pristine 2D GaN, with the Fermi level set to zero; (c) schematic structure of 6.25 at.% TM-doped 2D GaN; and (d) schematic structure of 9.375 at.% TM-doped 2D GaN. Green, gray, and red spheres denote Ga, N, and TM atoms, respectively.

the structural, magnetic, and electronic responses.

Tables 1 and 2 summarize the calculated TM-N bond length L, dopant-vacancy binding energy E_b, total magnetic moment M_{total}, dopant magnetic moment M_{TM}, and band gap E_g for the 6.25 at.% and 9.375 at.% TM-doped systems. At 6.25 at.% doping, the TM-N bond length decreases from 1.98 Å for Sc to 1.86 Å for V, remains at 1.86 Å for V, Cr, Mn, and Fe, decreases to 1.83 Å for Co and Ni, and then increases to 1.91 Å for Zn (Table 1). Thus, the Sc-N bond is the longest, whereas the Co-N and Ni-N bonds are the shortest. The proximity of these bond lengths to the sums of the corresponding covalent radii indicates that substitutional TM atoms form covalent bonds with neighboring N atoms. A similar trend is observed at 9.375 at.% doping (Table 2). The TM-N bond length decreases from 1.98 Å for Sc to 1.86 Å for Cr, remains at 1.86 Å for Cr, Mn, and Fe, reaches 1.83 Å for Co, and then increases to 1.90 Å for Zn. This concentration-independent trend indicates that local TM-N covalent bonding is retained as the dopant concentration increases from 6.25 at.% to 9.375 at.%.

Two distinct energetic quantities were evaluated. First, the dopant-vacancy binding energy E_b quantifies the energy gained when an isolated TM atom binds to a pre-existing Ga vacancy [44]. Under the definition in Eq. (1), a larger positive E_b indicates stronger binding. It was calculated as follows:

$$E_{\mathrm{b}} = E_{\mathrm{GaN}} + E_{\mathrm{atom}} - E_{\mathrm{total}} \quad (1)$$

where E_{GaN} is the total energy of the relaxed 2D GaN supercell containing a Ga vacancy, E_{atom} is the energy

Table 1. TM-N bond length L, dopant-vacancy binding energy E_b, total magnetic moment M_{total} per supercell, TM atomic magnetic moment M_{TM}, and band gap E_g for 6.25 at.% TM-doped 2D GaN.

	Sc	Ti	V	Cr	Mn	Fe	Co	Ni	Cu	Zn
L(Å)	1.98	1.91	1.86	1.86	1.86	1.86	1.83	1.83	1.86	1.91
E_b(eV)	27.58	28.53	25.27	21.10	20.60	21.68	21.15	19.40	14.84	13.45
$M_{total}(\mu_B)$	0	1.99	3.78	6.00	8.00	10.00	8.00	6.00	4.00	2.00
$M_{TM}(\mu_B)$	0	1.47	3.08	5.31	6.68	7.34	5.21	3.19	1.33	0.04
E_g(eV)	2.29	0.20	-	0.28	-	0.48	0.80	-	-	-

Table 2. TM-N bond length L, dopant-vacancy binding energy E_b, total magnetic moment M_{total} per supercell, TM atomic magnetic moment M_{TM}, and band gap E_g for 9.375 at.% TM-doped 2D GaN.

	Sc	Ti	V	Cr	Mn	Fe	Co	Ni	Cu	Zn
L(Å)	1.98	1.91	1.87	1.86	1.86	1.86	1.83	1.84	1.88	1.90
E_b(eV)	40.40	41.49	37.11	30.80	30.33	31.66	30.86	28.40	21.77	19.42
$M_{total}(\mu_B)$	0	3.00	5.78	9.00	12.00	15.00	12.00	9.00	5.33	2.99
$M_{TM}(\mu_B)$	0	2.33	4.97	7.97	10.05	11.03	7.84	4.76	1.77	0.11
E_g(eV)	2.39	0.27	-	-	0.05	0.23	0.55	-	-	-

of an isolated TM atom, and E_{total} is the total energy of the relaxed substitutional TM-doped supercell.

The dopant-vacancy binding energies range from 13.45 to 28.53 eV at 6.25 at.% and from 19.42 to 41.49 eV at 9.375 at.% (Tables 1 and 2). Ti has the largest value at both concentrations, indicating the strongest calculated association between the dopant and a pre-existing Ga vacancy among the screened elements. Zn has the smallest value, although its positive binding energy still indicates exothermic trapping at the vacancy under the definition used here. Thus, E_b characterizes local dopant-vacancy binding and should not be interpreted as the substitutional formation energy.

Second, the substitutional defect formation energy E_f measures the thermodynamic cost of replacing a Ga atom with a TM atom relative to the selected atomic reservoirs [45]. Unlike E_b, a lower E_f indicates more favorable dopant incorporation. It was calculated as follows:

$$E_{\text{f}} = E_{\text{doped}} + \mu_{\text{Ga}} - E_{\text{perfect}} - \mu_{\text{TM}} \qquad (2)$$

where E_{doped} is the total energy of the TM-doped 2D GaN supercell, E_{perfect} is the total energy of the pristine supercell of the same size, and μ_{Ga} and μ_{TM} are the chemical potentials of Ga and the TM species, respectively. The substitutional defect formation energies of the 6.25 at.% and 9.375 at.% systems are shown in Figure 2. The differences indicate that dopant incorporation depends strongly on the TM species. Sc and Ti have comparatively low formation energies at both concentrations, indicating more favorable substitution than for most other TM species under the same chemical-potential conditions.

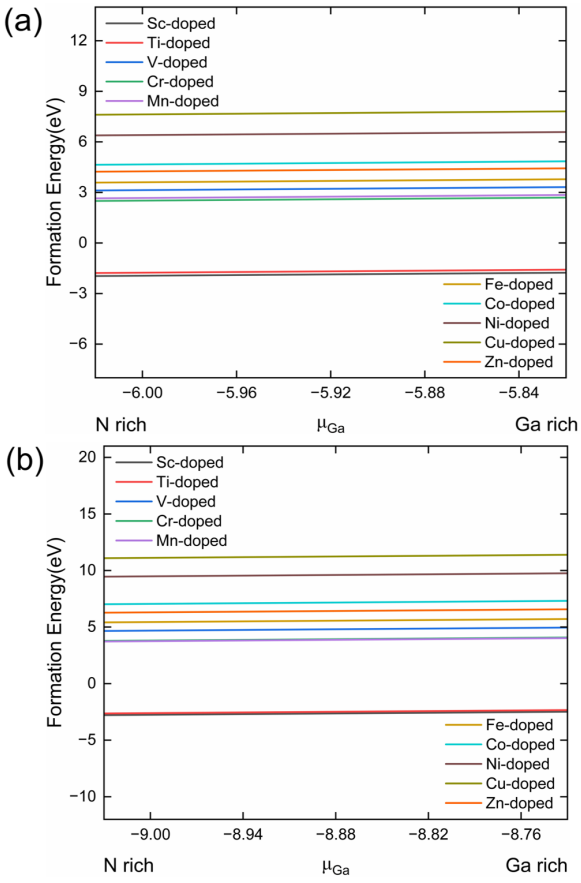

Figure 2. Substitutional defect formation energies of TM-doped 2D GaN: (a) 6.25 at.%; and (b) 9.375 at.%.

Pristine 2D GaN is non-magnetic, whereas transition-metal doping has been widely demonstrated to introduce finite magnetic moments in two-dimensional materials [46]. At 6.25 at.% doping, Ti-Zn substitution produces total magnetic moments of 1.99, 3.78, 6.00, 8.00, 10.00, 8.00, 6.00, 4.00, and 2.00 μ_B, respectively, whereas Sc substitution remains non-magnetic (Table 1). At 9.375 at.% doping, Sc substitution again remains non-magnetic, while Ti-Zn substitution produces total magnetic moments of 3.00, 5.78, 9.00, 12.00, 15.00, 12.00, 9.00, 5.33, and 2.99 μ_B, respectively (Table 2).

The dopant contribution to the total magnetic moment follows two regimes. For Ti-Fe substitution, the dopant atom contributes more than 70% of the total magnetic moment, with local TM moments of 1.47, 3.08, 5.31, 6.68, and 7.34 μ_B at 6.25 at.% and 2.33, 4.97, 7.97, 10.05, and 11.03 μ_B at 9.375 at.%. For Co-Zn substitution, the dopant contribution is lower than 70%, indicating a larger role for neighboring N atoms in the magnetic response. The local Co-Zn moments are 5.21, 3.19, 1.33, and 0.04 μ_B at 6.25 at.% and 7.84, 4.76, 1.77, and 0.11 μ_B at 9.375 at.%, respectively.

Spin-density distributions were analyzed to clarify the origin of the magnetic moments. Figures 3 and 4 show the spin-density distributions of 6.25 at.% and 9.375 at.% Ti-Zn-doped 2D GaN. For Ti-Fe substitution, the spin density is mainly localized around the impurity atom, consistent with the dominant dopant contribution listed in Tables 1 and 2. For Co-Cu substitution, spin polarization appears on both the dopant and neighboring N atoms, indicating stronger dopant-N magnetic coupling. For Zn substitution, the Zn atom contributes only a small local moment, but the neighboring N atoms become spin polarized, giving total magnetic moments of 2.00 μ_B at 6.25 at.% and 2.99 μ_B at 9.375 at.%. These features indicate a transition from dopant-dominated magnetism in the Ti-Fe systems to greater ligand involvement in the Co-, Ni-, Cu-, and Zn-doped systems.

Band-structure calculations were used to distinguish non-magnetic, magnetic semiconducting, metallic, and half-metallic behavior [47]. Figures 5 and 6 show the spin-resolved band structures of TM-doped 2D GaN at 6.25 at.% and 9.375 at.%, respectively. For Sc-doped 2D GaN, the spin-up and spin-down bands overlap at both concentrations, confirming the non-magnetic character. For Ti-Zn substitution, the spin-up and spin-down bands are split, consistent with the finite magnetic moments. At 6.25 at.% doping, Sc-, Ti-, Cr-, Fe-, and Co-doped systems are semiconductors with band gaps of 2.29, 0.20, 0.28, 0.48, and 0.80 eV, respectively. Sc, Ti, Cr, and Co have indirect band gaps, whereas Fe has a direct gap at Γ. The V-doped system is metallic because both spin channels cross the Fermi level. Mn-, Ni-, Cu-, and Zn-doped systems are half-metallic because one spin channel is metallic while the other remains semiconducting, producing complete spin polarization at the Fermi level.

At 9.375 at.% doping, Sc-, Ti-, Mn-, Fe-, and Co-doped systems remain semiconducting, with band gaps of 2.39, 0.27, 0.05, 0.23, and 0.55 eV, respectively (Figure 6 and Table 2). Sc, Ti, Mn, and Co exhibit indirect band gaps, while Fe again shows a direct gap at Γ. The V- and Cu-doped systems are metallic, whereas Cr-, Ni-, and Zn-doped systems are half-metallic. Increasing the dopant concentration therefore changes the electronic classification of selected dopants, but Co substitution remains a magnetic semiconductor at both concentrations.

For semiconductor spintronic operation, the magnetic semiconductor should retain a band gap larger than 0.50 eV to suppress thermally generated intrinsic carriers. Under this criterion, 6.25 at.% and 9.375 at.% Co-doped 2D GaN are the only screened systems that simultaneously exhibit structural stability, magnetic behavior, and suitable semiconductor band gaps. These two Co-doped systems were therefore selected for the subsequent strain analysis.

Analyses of the total and projected densities of states (TDOS and PDOS) further support the magnetic and bonding interpretations. Figures 7 and 8 show the TDOS and PDOS of 6.25 at.% and 9.375 at.% TM-doped 2D GaN, respectively. For Ti-Zn substitution, the spin-up and spin-down density-of-states profiles are asymmetric, confirming the magnetic character of these doped systems. The PDOS reveals strong hybridization between N 2p and TM 3d orbitals near the Fermi level, consistent with covalent TM-N interactions. For example, in 6.25 at.% Co-doped 2D GaN, the Co 3d states overlap strongly with the neighboring N 2p states near the Fermi level, particularly in the spin-polarized channels. This hybridization contributes to spin-polarized electronic states while maintaining a finite semiconductor band gap and is consistent with the relatively high Co dopant-vacancy binding energy.

The screening results identify 6.25 at.% and 9.375 at.% Co-doped 2D GaN as the most suitable magnetic semiconductor candidates because they combine

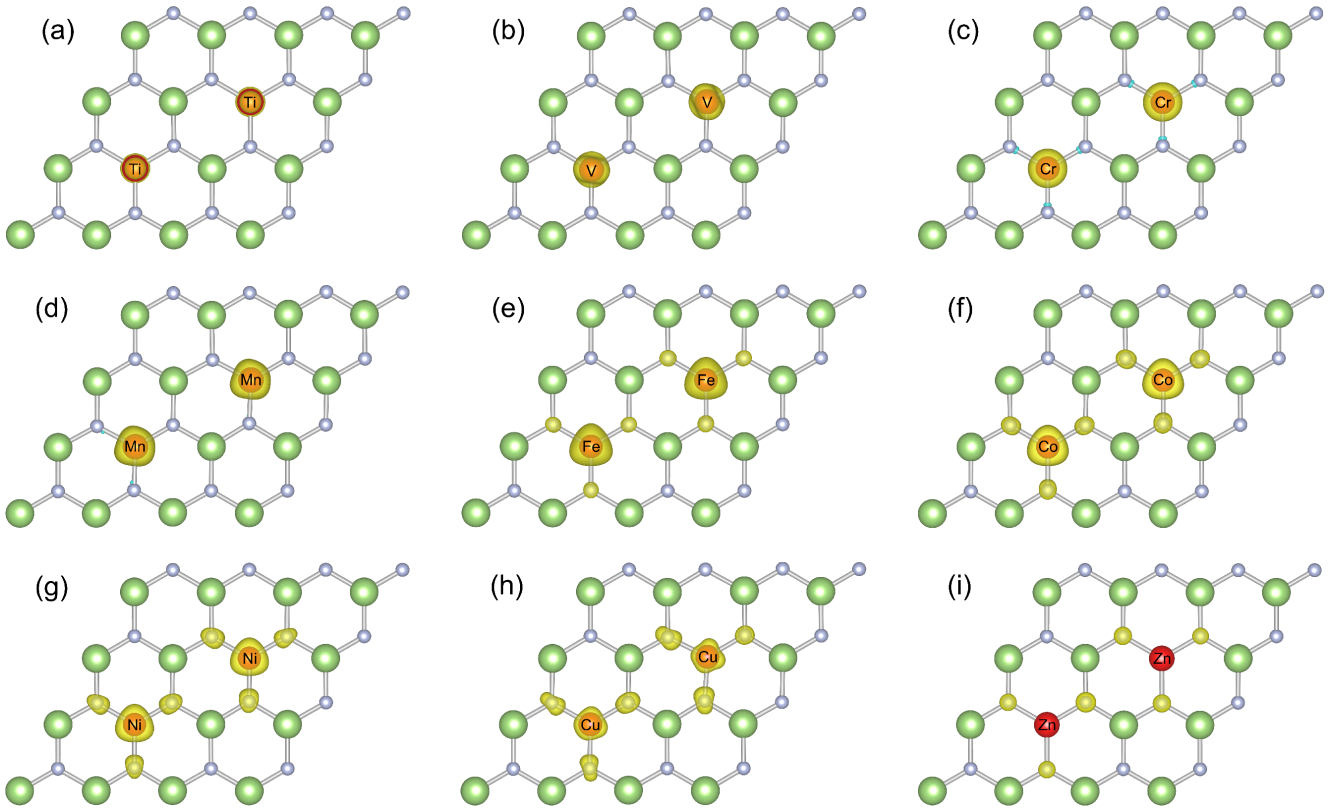

Figure 3. Spin-density distributions of 6.25 at.% TM-doped 2D GaN. The isosurface value is 0.02 e Å^{-3}. Yellow and cyan indicate net spin-up and spin-down polarization, respectively.

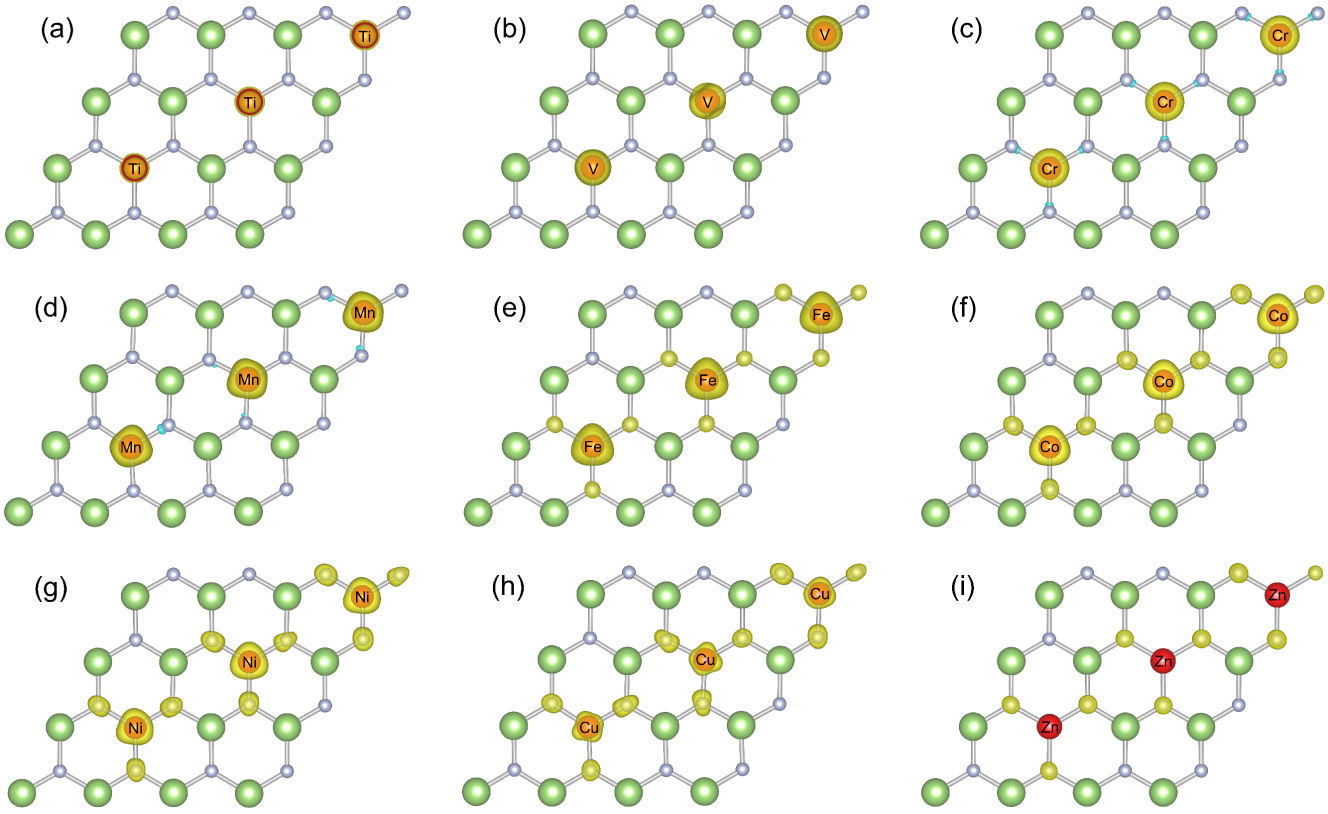

Figure 4. Spin-density distributions of 9.375 at.% TM-doped 2D GaN. The isosurface value is 0.02 e Å^{-3}. Yellow and cyan indicate net spin-up and spin-down polarization, respectively.

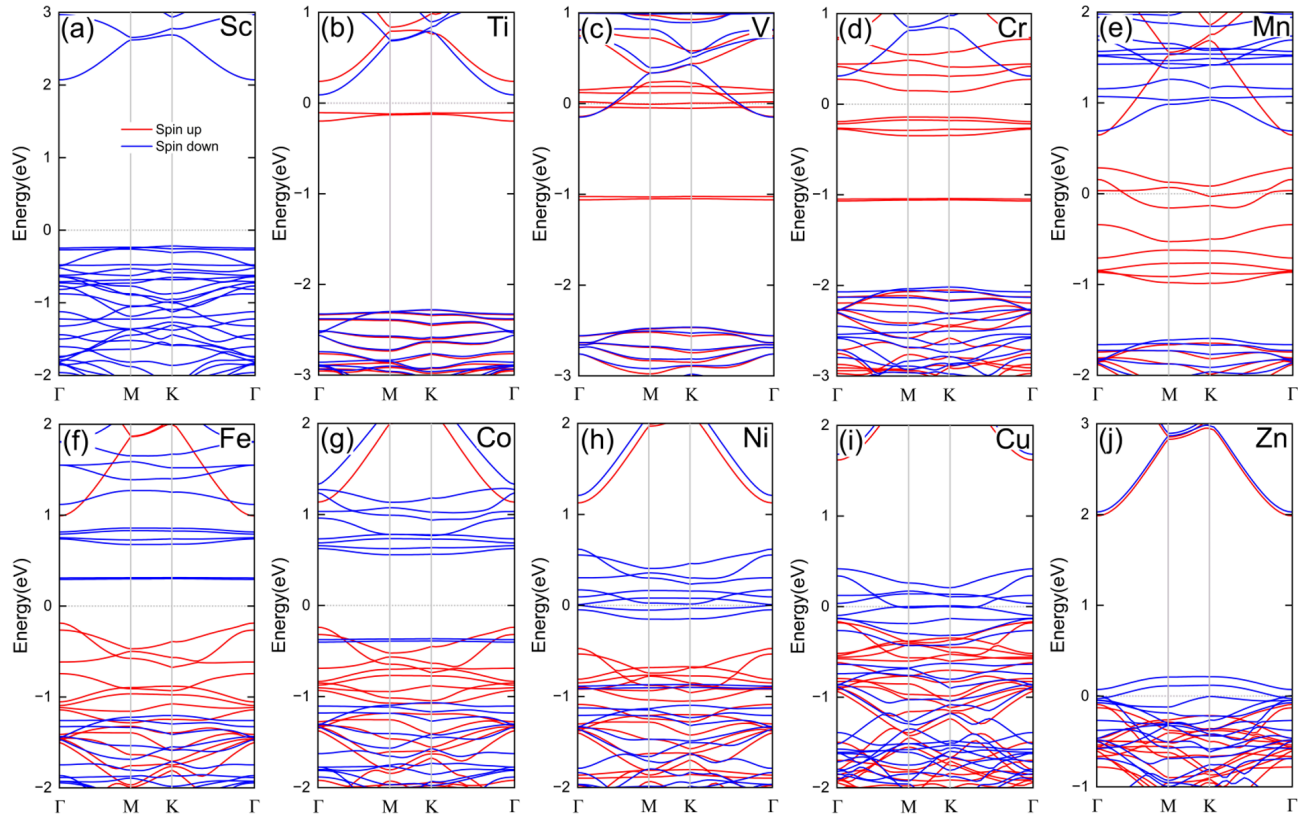

Figure 5. Band structures of 6.25 at.% TM-doped 2D GaN: (a) Sc; (b) Ti; (c) V; (d) Cr; (e) Mn; (f) Fe; (g) Co; (h) Ni; (i) Cu; and (j) Zn. Red and blue lines denote spin-up and spin-down channels, respectively. The Fermi level is set to zero.

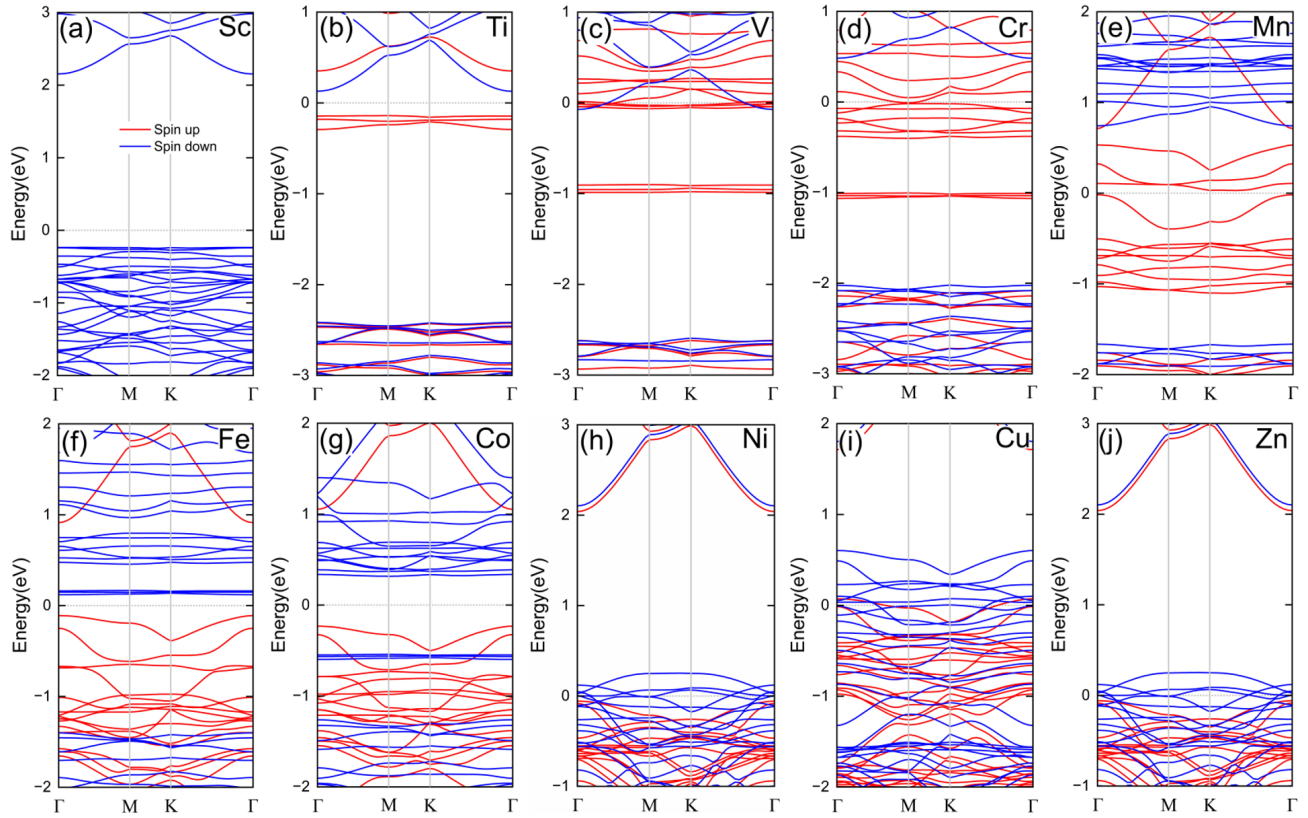

Figure 6. Band structures of 9.375 at.% TM-doped 2D GaN: (a) Sc; (b) Ti; (c) V; (d) Cr; (e) Mn; (f) Fe; (g) Co; (h) Ni; (i) Cu; and (j) Zn. Red and blue lines denote spin-up and spin-down channels, respectively. The Fermi level is set to zero.

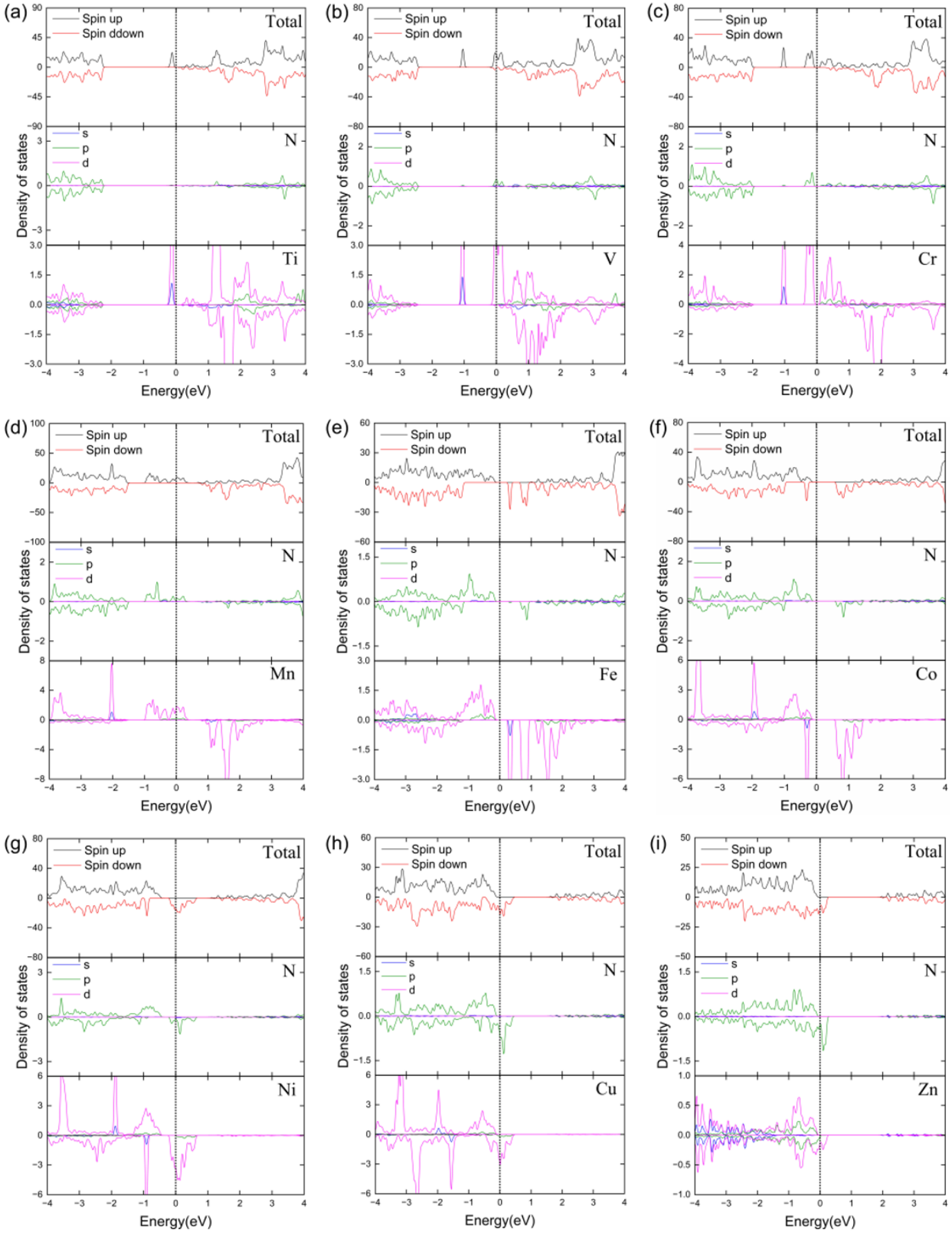

Figure 7. TDOS and PDOS of 6.25 at.% TM-doped 2D GaN. The Fermi level is set to zero.

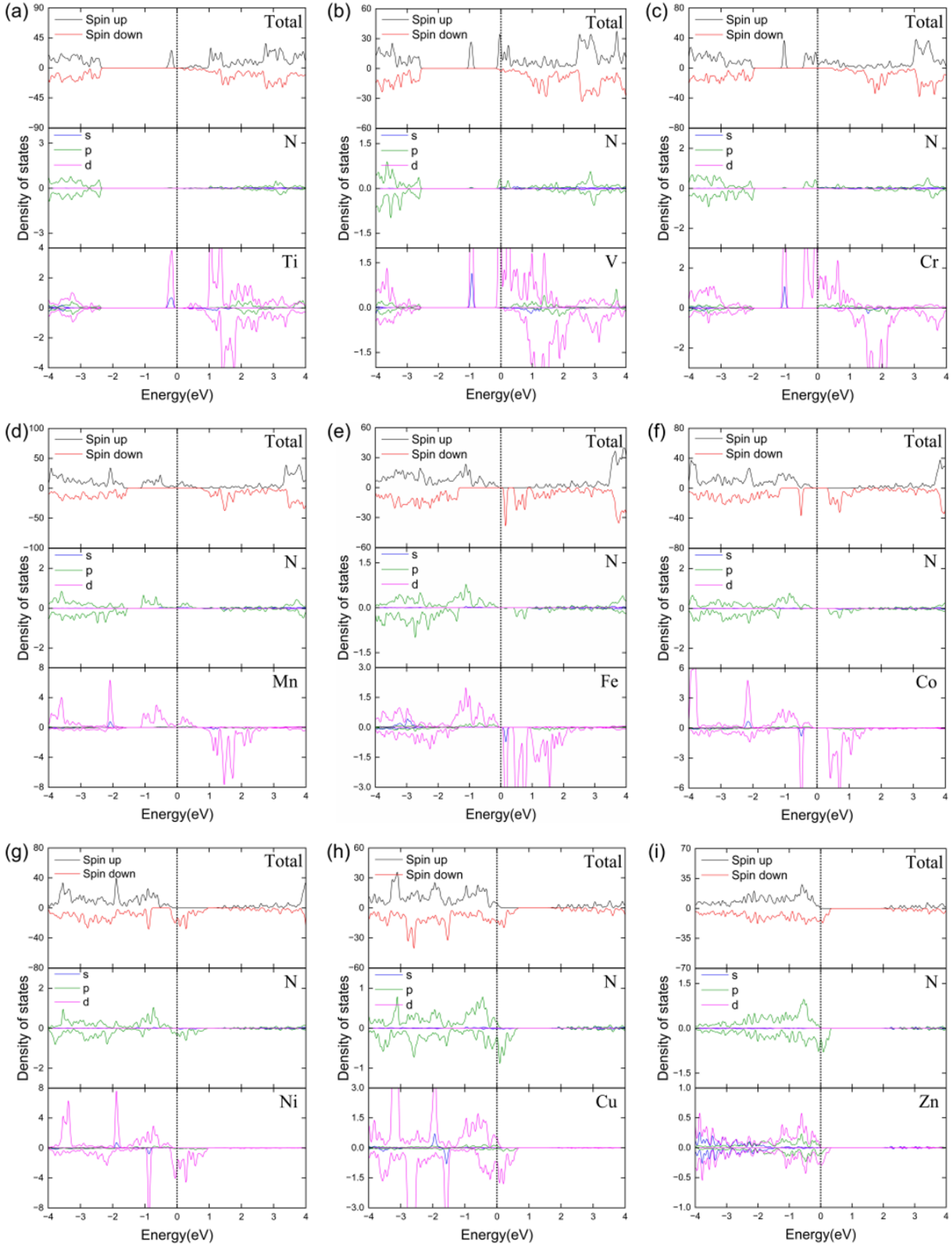

Figure 8. TDOS and PDOS of 9.375 at.% TM-doped 2D GaN. The Fermi level is set to zero.

stable structures, finite magnetism, and band gaps above 0.50 eV. The next question is whether their band gaps can be tuned without losing these favorable properties. To address this question, biaxial strains from -3% to 3% were applied to both Co-doped systems.

Biaxial strain was introduced by changing the in-plane lattice parameters along the x and y directions. The strain δ was defined as follows:

$$\delta = \frac{a - a_0}{a_0} \times 100\% \quad (3)$$

Figure 9 shows the schematic structure of Co-doped 2D GaN under biaxial strain.

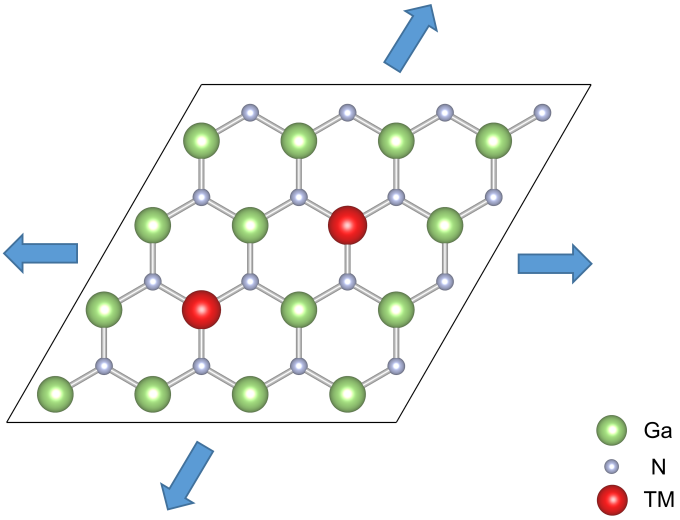

Figure 9. Schematic structure of Co-doped 2D GaN under biaxial strain.

Tables 3 and 4 summarize the TM-N bond length L, strain energy ΔE_s, total magnetic moment M_{total}, dopant magnetic moment M_{TM}, and band gap E_g of 6.25 at.% and 9.375 at.% Co-doped 2D GaN under -3% to 3% biaxial strain.

The Co-N bond length increases monotonically with increasing strain. For 6.25 at.% Co-doped 2D GaN, L increases from 1.77 Å under -3% compressive strain to 1.89 Å under 3% tensile strain. For 9.375 at.% Co-doped 2D GaN, L increases from 1.78 to 1.89 Å over the same strain range. This trend directly reflects in-plane lattice contraction under compressive strain and lattice expansion under tensile strain.

The strain energy $\Delta E_s = E_{\text{strained}} - E_{\text{relaxed}}$, where E_{strained} and E_{relaxed} are the total energies of the strained and fully relaxed supercells respectively, was calculated to evaluate the stability of the strained structures. Figures 10 (a) and (b) show the

Table 3. TM-N bond length L, strain energy ΔE_s, total magnetic moment M_{total} per supercell, TM atomic magnetic moment M_{TM}, and band gap E_g for 6.25 at.% Co-doped 2D GaN under -3% to 3% biaxial strain.

Strain(%)	-3	-2	-1	0	1	2	3
L(Å)	1.77	1.79	1.81	1.83	1.85	1.87	1.89
ΔE_s(eV)	1.51	0.59	0.10	0.00	0.26	0.84	1.70
$M_{total}(\mu_B)$	8.00	8.00	8.00	8.00	8.00	8.00	8.00
$M_{TM}(\mu_B)$	5.20	5.20	5.21	5.21	5.21	5.20	5.20
E_g(eV)	0.57	0.65	0.73	0.80	0.86	0.89	0.86

Table 4. TM-N bond length L, strain energy ΔE_s, total magnetic moment M_{total} per supercell, TM atomic magnetic moment M_{TM}, and band gap E_g for 9.375 at.% Co-doped 2D GaN under -3% to 3% biaxial strain.

Strain(%)	-3	-2	-1	0	1	2	3
L(Å)	1.78	1.79	1.81	1.83	1.85	1.87	1.89
ΔE_s(eV)	1.39	0.51	0.06	0.00	0.28	0.88	1.76
$M_{total}(\mu_B)$	12.00	12.00	12.00	12.00	12.00	12.00	12.00
$M_{TM}(\mu_B)$	7.43	7.84	7.85	7.84	7.85	7.84	7.84
E_g(eV)	0.22	0.39	0.47	0.55	0.62	0.64	0.65

strain-energy curves for 6.25 at.% and 9.375 at.% Co-doped 2D GaN, respectively. In both systems, the strain energy increases as the magnitude of either compressive or tensile strain increases away from the relaxed state. This nearly symmetric increase indicates that the structures remain within the elastic deformation regime over the -3% to 3% strain range. At -3% compressive strain, the strain energies are 1.51 eV and 1.39 eV for the 6.25 at.% and 9.375 at.% systems, respectively. At 3% tensile strain, they increase to 1.70 eV and 1.76 eV, respectively, indicating that tensile strain imposes a slightly higher energetic cost at the largest strain magnitude considered here.

Biaxial strain changes the band gaps of both Co-doped systems while preserving magnetic order. Figures 11 (a) and (b) show the band-gap evolution of 6.25 at.% and 9.375 at.% Co-doped 2D GaN, respectively, and the corresponding values are listed in Tables 3 and 4. For 6.25 at.% Co-doped 2D GaN, the band gap increases from 0.57 eV at -3% strain to a maximum of 0.89 eV at 2% tensile strain, and then slightly decreases to 0.86 eV at 3% tensile strain. For 9.375 at.% Co-doped 2D GaN, the band gap increases monotonically from 0.22 eV at -3% strain to 0.65 eV at 3% tensile strain. These trends show that strain can tune the electronic gap over a practically relevant range without eliminating magnetism.

Spin-resolved band structures under biaxial strain are shown in Figures 12 and 13. For 6.25 at.% Co-doped 2D

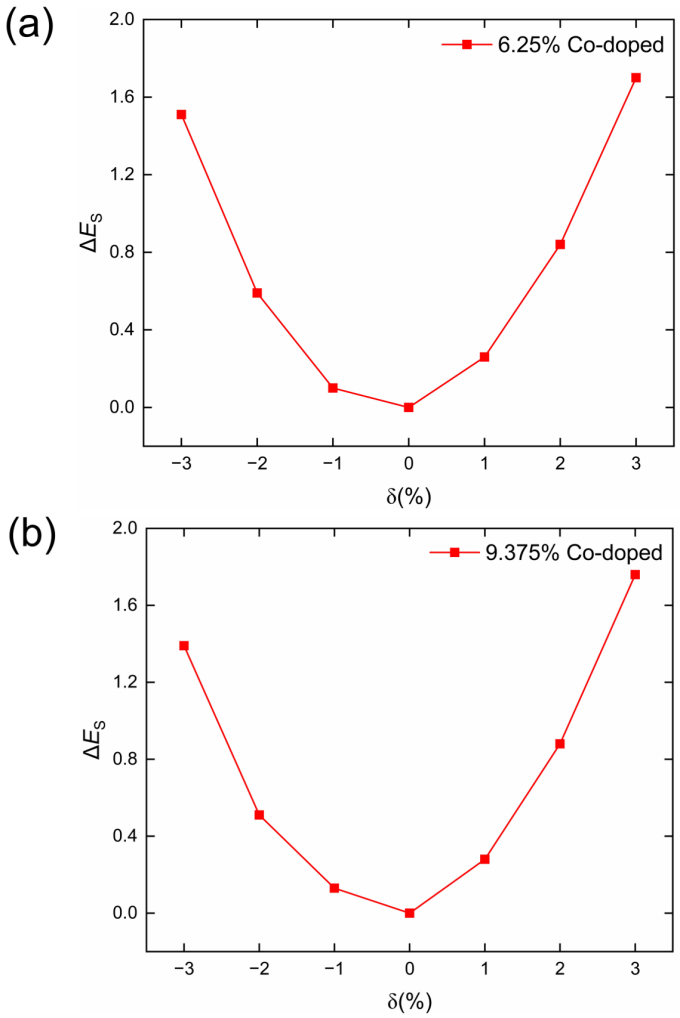

Figure 10. Strain-energy curves of Co-doped 2D GaN under -3% to 3% biaxial strain: (a) 6.25 at.%; and (b) 9.375 at.%.

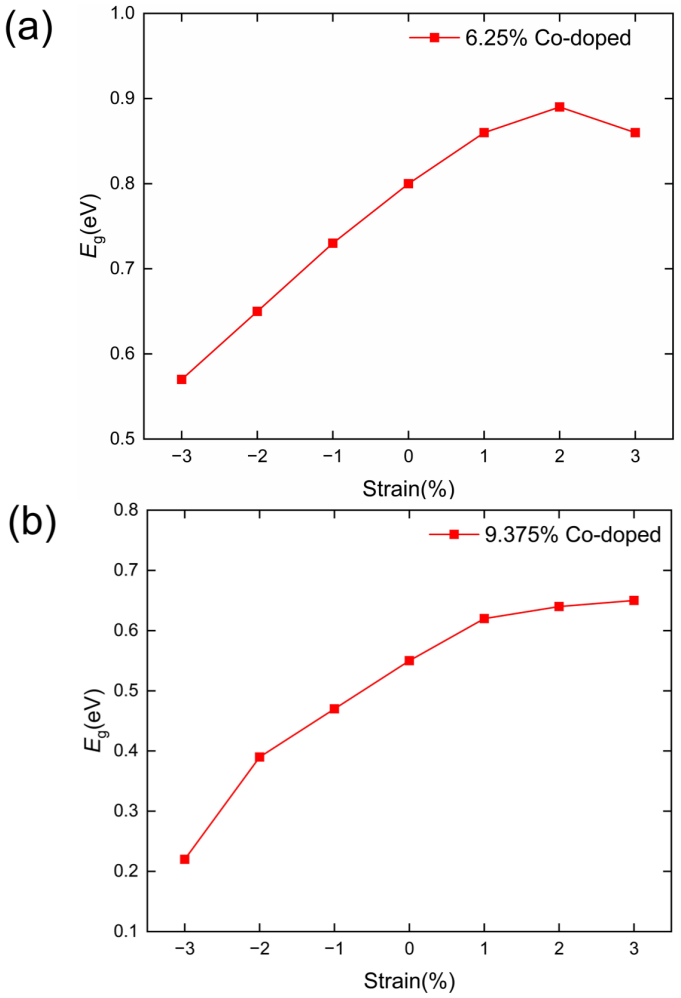

Figure 11. Band-gap evolution of Co-doped 2D GaN under -3% to 3% biaxial strain: (a) 6.25 at.%; and (b) 9.375 at.%.

GaN, all strained structures from -3% to 3% remain magnetic semiconductors, with band gaps of 0.57, 0.65, 0.73, 0.80, 0.86, 0.89, and 0.86 eV, respectively. The systems retain indirect band gaps from -3% to 2% strain, whereas the 3% tensile case changes to a direct band gap. For 9.375 at.% Co-doped 2D GaN, all strained structures also remain magnetic semiconductors, with band gaps of 0.22, 0.39, 0.47, 0.55, 0.62, 0.64, and 0.65 eV from -3% to 3% strain. However, only the 0% to 3% strain cases satisfy the > 0.50 eV band-gap criterion used here. The 9.375 at.% system therefore requires neutral or tensile strain to retain a gap large enough for the targeted spintronic condition.

Taken together, the strain calculations show that 6.25 at.% Co-doped 2D GaN retains structural stability, magnetism, and a band gap above 0.50 eV throughout the -3% to 3% strain range. The 9.375 at.% Co-doped system meets the same criterion from 0% to 3% strain. In both systems, the band gap changes systematically with strain, and 3% tensile strain changes the 6.25 at.% system from an indirect- to a direct-gap semiconductor. These results indicate that moderate biaxial strain can tune the electronic structure of Co-doped 2D GaN while preserving its magnetic-semiconductor character.

4 Conclusion

This study used first-principles calculations to examine how 3d transition-metal substitution (TM = Sc-Zn) and biaxial strain modulate the structural, magnetic, and electronic properties of 2D GaN. Among the dopants considered, Co substitution provides the most suitable balance of structural stability, magnetic order, and semiconductor band gap. The 6.25 at.% and 9.375 at.% Co-doped systems have magnetic moments of 8.00 and 12.00 μ_B per supercell and band gaps of 0.80 and 0.55 eV, respectively. Under biaxial strain, 6.25 at.% Co-doped 2D GaN retains a magnetic-semiconductor state with a band gap larger than 0.50 eV from -3% to 3%, whereas the 9.375

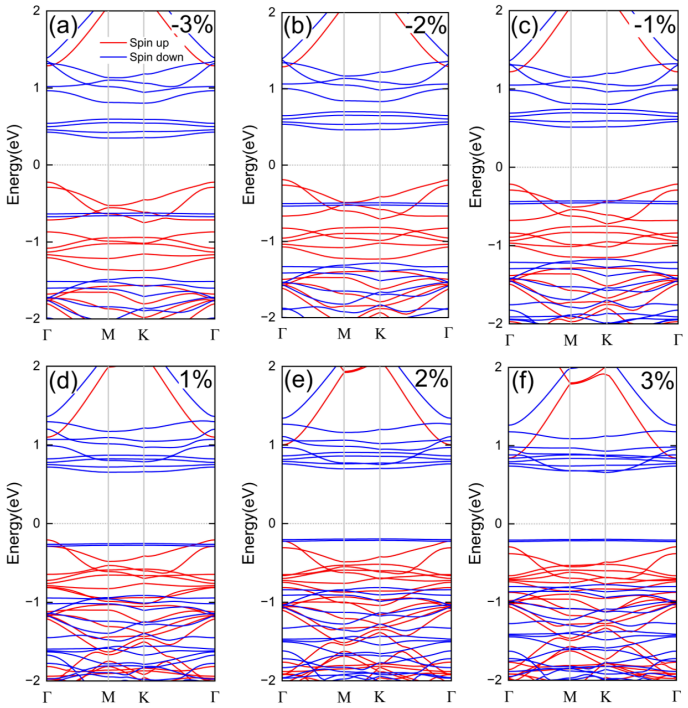

Figure 12. Band structures of 6.25 at.% Co-doped 2D GaN under -3% to 3% biaxial strain: (a) -3%; (b) -2%; (c) -1%; (d) 1%; (e) 2%; and (f) 3%. Red and blue lines denote spin-up and spin-down channels, respectively. The Fermi level is set to zero.

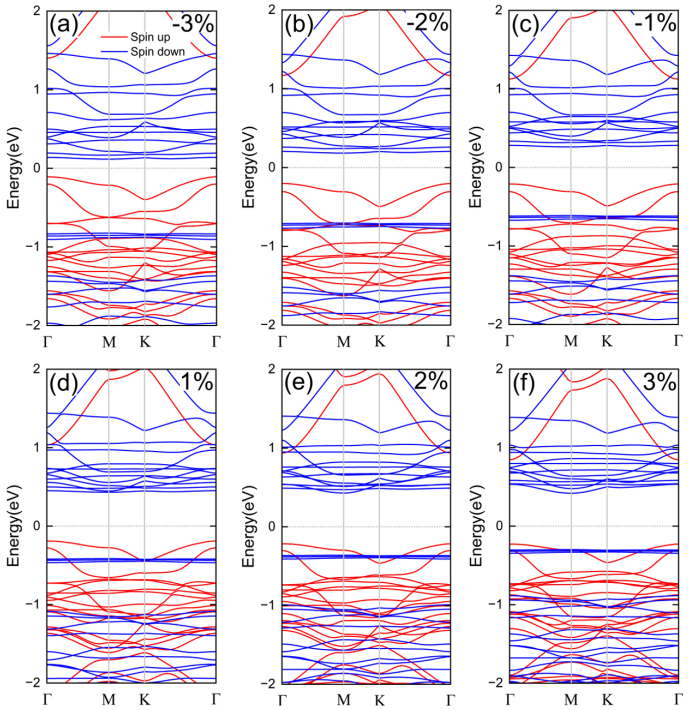

Figure 13. Band structures of 9.375 at.% Co-doped 2D GaN under -3% to 3% biaxial strain: (a) -3%; (b) -2%; (c) -1%; (d) 1%; (e) 2%; and (f) 3%. Red and blue lines denote spin-up and spin-down channels, respectively. The Fermi level is set to zero.

at.% system satisfies this criterion from 0% to 3%. The 6.25 at.% system reaches a maximum band gap of 0.89 eV at 2% tensile strain and changes from an indirect to a direct band gap at 3% tensile strain. These first-principles results suggest that Co substitution combined with moderate biaxial strain may provide a useful theoretical design principle for tuning the properties of monolayer GaN. Experimental validation and higher-level electronic-structure calculations are needed before its feasibility for spintronic devices can be established.

Data Availability Statement

Data will be made available on request.

Funding

This work was supported by the Natural Science Foundation of Jiangsu Province, China under Grant BK20241056, and by the Natural Science Foundation of the Jiangsu Higher Education Institutions of China under Grant 24KJB460012.

Conflicts of Interest

The authors declare no conflicts of interest.

AI Use Statement

The authors declare that no generative AI was used in the preparation of this manuscript.

Ethical Approval and Consent to Participate

Not applicable.

References

[1] Bhatti, S., Sbiaa, R., Hirohata, A., Ohno, H., Fukami, S., & Piramanayagam, S. N. (2017). Spintronics based random access memory: a review. *Materials today, 20*(9), 530-548. [CrossRef]

[2] Gupta, R., Bouard, C., Kammerbauer, F., Ledesma-Martin, J. O., Bose, A., Kononenko, I., ... & Kläui, M. (2025). Harnessing orbital Hall effect in spin-orbit torque MRAM. *Nature Communications, 16*(1), 130. [CrossRef]

[3] Ghising, P., Biswas, C., & Lee, Y. H. (2023). Graphene spin valves for spin logic devices. *Advanced Materials, 35*(23), 2209137. [CrossRef]

[4] Li, M., Li, C., Xu, X., Wang, M., Zhu, Z., Meng, K., ... & Jiang, Y. (2023). An ultrathin flexible programmable spin logic device based on spin–orbit torque. *Nano Letters, 23*(9), 3818-3825. [CrossRef]

[5] Ahn, E. C. (2020). 2D materials for spintronic devices. *npj 2D Materials and Applications, 4*(1), 17. [CrossRef]

[6] Meng, K., Li, M., Guo, L., Zhang, R., Guo, A., Liu, M., ... & Sun, X. (2025). Room-Temperature Organic Spintronic Devices with Wide Range Magnetocurrent Tuning and Multifunctionality via Electro-Optical Compensation Strategy. *Advanced Materials, 37*(11), 2417995. [CrossRef]

[7] González, V. H., Litvinenko, A., Kumar, A., Khymyn, R., & Åkerman, J. (2024). Spintronic devices as next-generation computation accelerators. *Current Opinion in Solid State and Materials Science, 31*, 101173. [CrossRef]

[8] Mi, M., Xiao, H., Yu, L., Zhang, Y., Wang, Y., Cao, Q., & Wang, Y. (2023). Two-dimensional magnetic materials for spintronic devices. *Materials Today Nano, 24*, 100408. [CrossRef]

[9] Chen, B., Zeng, M., Khoo, K. H., Das, D., Fong, X., Fukami, S., ... & Ter Lim, S. (2023). Spintronic devices for high-density memory and neuromorphic computing–A review. *Materials Today, 70*, 193-217. [CrossRef]

[10] Li, B., Xing, T., Zhong, M., Huang, L., Lei, N., Zhang, J., ... & Wei, Z. (2017). A two-dimensional Fe-doped SnS2 magnetic semiconductor. *Nature communications, 8*(1), 1958. [CrossRef]

[11] Liu, Y., Duan, X., Huang, Y., & Duan, X. (2018). Two-dimensional transistors beyond graphene and TMDCs. *Chemical Society Reviews, 47*(16), 6388-6409. [CrossRef]

[12] Li, Y., Huang, S., Peng, S., Jia, H., Pang, J., Ibarlucea, B., ... & Cuniberti, G. (2023). Toward smart sensing by MXene. *Small, 19*(14), 2206126. [CrossRef]

[13] Solangi, N. H., Karri, R. R., Mazari, S. A., Mubarak, N. M., Jatoi, A. S., Malafaia, G., & Azad, A. K. (2023). MXene as emerging material for photocatalytic degradation of environmental pollutants. *Coordination Chemistry Reviews, 477*, 214965. [CrossRef]

[14] Wang, J., Ma, F., Liang, W., & Sun, M. (2017). Electrical properties and applications of graphene, hexagonal boron nitride (h-BN), and graphene/h-BN heterostructures. *Materials Today Physics, 2*, 6-34. [CrossRef]

[15] Cao, Z., Zhang, H., Song, B., Xiong, D., Tao, S., Deng, W., ... & Ji, X. (2023). Angstrom-level ionic sieve 2D-MOF membrane for high power aqueous zinc anode. *Advanced Functional Materials, 33*(28), 2300339. [CrossRef]

[16] Lin, Y. C., Torsi, R., Younas, R., Hinkle, C. L., Rigosi, A., Hill, H. M., ... & Robinson, J. A. (2023). Recent advances in 2D material theory, synthesis, properties, and applications. *ACS nano, 17*(11), 9694. [CrossRef]

[17] Cao, W., Jiang, J., Xie, X., Pal, A., Chu, J. H., Kang, J., & Banerjee, K. (2018). 2-D layered materials for next-generation electronics: Opportunities and challenges. *IEEE Transactions on Electron Devices, 65*(10), 4109-4121. [CrossRef]

[18] Zhang, X., Hou, L., Ciesielski, A., & Samorì, P. (2016). 2D materials beyond graphene for high-performance energy storage applications. *Advanced Energy Materials, 6*(23), 1600671. [CrossRef]

[19] Gao, L. (2017). Flexible device applications of 2D semiconductors. *Small, 13*(35), 1603994. [CrossRef]

[20] Yu, S., Wu, X., Wang, Y., Guo, X., & Tong, L. (2017). 2D materials for optical modulation: challenges and opportunities. *Advanced Materials, 29*(14), 1606128. [CrossRef]

[21] Chen, L. X., Chen, Z. W., Jiang, M., Lu, Z., Gao, C., Cai, G., & Singh, C. V. (2021). Insights on the dual role of two-dimensional materials as catalysts and supports for energy and environmental catalysis. *Journal of Materials Chemistry A, 9*(4), 2018-2042. [CrossRef]

[22] Zhang, F., Li, C., Li, Z., Dong, L., & Zhao, J. (2023). Recent progress in three-terminal artificial synapses based on 2D materials: from mechanisms to applications. *Microsystems & Nanoengineering, 9*(1), 16. [CrossRef]

[23] Wen, X., Lei, B., Zhang, L., & Lu, H. (2025). Tuning of the Electronic and Magnetic Properties of GaN Monolayers via Doping with Lanthanide Atoms and by Applying Biaxial Strain. *Nanomaterials, 15*(17), 1331. [CrossRef]

[24] Chen, Y., Liu, J., Liu, K., Si, J., Ding, Y., Li, L., ... & Fu, L. (2019). GaN in different dimensionalities: Properties, synthesis, and applications. *Materials Science and Engineering: R: Reports, 138*, 60-84. [CrossRef]

[25] Al Balushi, Z. Y., Wang, K., Ghosh, R. K., Vilá, R. A., Eichfeld, S. M., Caldwell, J. D., ... & Robinson, J. A. (2016). Two-dimensional gallium nitride realized via graphene encapsulation. *Nature materials, 15*(11), 1166-1171. [CrossRef]

[26] Sanders, N., Bayerl, D., Shi, G., Mengle, K. A., & Kioupakis, E. (2017). Electronic and optical properties of two-dimensional GaN from first-principles. *Nano letters, 17*(12), 7345-7349. [CrossRef]

[27] Wang, Z., Wang, G., Liu, X., Wang, S., Wang, T., Zhang, S., ... & Zhang, L. (2021). Two-dimensional wide band-gap nitride semiconductor GaN and AlN materials: properties, fabrication and applications. *Journal of Materials Chemistry C, 9*(48), 17201-17232. [CrossRef]

[28] Kecik, D., Onen, A., Konuk, M., Gürbüz, E., Ersan, F., Cahangirov, S., ... & Ciraci, S. (2018). Fundamentals, progress, and future directions of nitride-based semiconductors and their composites in two-dimensional limit: A first-principles perspective to recent synthesis. *Applied Physics Reviews, 5*(1). [CrossRef]

[29] Onen, A., Kecik, D., Durgun, E., & Ciraci, S. (2016). GaN: From three-to two-dimensional single-layer crystal and its multilayer van der Waals solids. *Physical Review B, 93*(8), 085431. [CrossRef]

[30] Kadioglu, Y., Ersan, F., Kecik, D., Aktürk, O. Ü., Aktürk, E., & Ciraci, S. (2018). Chemical and substitutional doping, and anti-site and vacancy formation in monolayer AlN and GaN. *Physical Chemistry Chemical Physics, 20*(23), 16077-16091. [CrossRef]

[31] Zhao, Q., Xiong, Z., Qin, Z., Chen, L., Wu, N., & Li, X. (2016). Tuning magnetism of monolayer GaN by vacancy and nonmagnetic chemical doping. *Journal of Physics and Chemistry of Solids, 91*, 1-6. [CrossRef]

[32] Jin, X. W., Xie, Y., Han, W., Chen, Z. Y., Xiao, X. S., Hao, J. Y., ... & Song, Y. L. (2024). Biaxial strain-modulated power conversion efficiency, electronic structures, and optical properties of type-II MoS2/BC6N vdW heterostructure: A density functional theory study. *Materials Today Communications, 40*, 110012. [CrossRef]

[33] Li, X., Liu, M., Guo, M., Niu, C., He, H., Liu, Z., ... & Sui, J. (2023). Tailoring band structure and Ge precipitates through Er and Sb/Bi co-doping to realize high thermoelectric performance in GeTe. *Chemical Engineering Journal, 474*, 145820. [CrossRef]

[34] Wang, J., Guan, L., Yuan, S., Zhang, J., Zhao, C., Hu, X., ... & He, Y. (2023). Greatly boosted photocatalytic N2-to-NH3 conversion by bismuth doping in CdMoO4: Band structure engineering and N2 adsorption modification. *Separation and Purification Technology, 314*, 123554. [CrossRef]

[35] Wang, K., Yang, S., Ren, K., Wei, Y., Liu, H., & Zhang, G. (2026). Phonons regulate covalency: a new way to modulate the magnetism and Curie temperature of CrI3. *Physical Chemistry Chemical Physics, 28*(18), 11363-11369. [CrossRef]

[36] Guo-Xiang, C., Xiao-Bo, F., Si-Qi, L., & Jian-Min, Z. (2019). First-principles study of magnetic properties of alkali metals and alkaline earth metals doped two-dimensional GaN materials. *Acta Physica Sinica, 68*(23), 237303. [CrossRef]

[37] Liu, P., Peng, Y., Huang, Q., Zhou, Z., Shao, C., Guo, Y., & Han, R. (2023). First-principles investigates on the electronic structure and magnetic properties of V-, Cr-, Mn-doped two-dimensional Ga_2O_3. *Physics Letters A, 491*, 129211. [CrossRef]

[38] Aldbea, F. W., Vázquez Vázquez, C., Othman, U. A., Sharma, A., Boukhachemd, A., Mailoude, O. M., ... & Singh, P. K. (2024). Structural and optical properties of Iodine doped zinc oxide nanoparticles. *Journal of Materials Science: Materials in Electronics, 35*(7), 459. [CrossRef]

[39] Hafner, J. (2008). Ab-initio simulations of materials using VASP: Density-functional theory and beyond. *Journal of computational chemistry, 29*(13), 2044-2078. [CrossRef]

[40] Blöchl, P. E. (1994). Projector augmented-wave method. *Physical review B, 50*(24), 17953. [CrossRef]

[41] Perdew, J. P., Burke, K., & Ernzerhof, M. (1996). Generalized gradient approximation made simple. *Physical review letters, 77*(18), 3865. [CrossRef]

[42] Hussain, F., Cai, Y. Q., Khan, M. J. I., Imran, M., Rashid, M., Ullah, H., ... & Ahmad, S. A. (2015). Enhanced ferromagnetic properties of Cu doped two-dimensional GaN monolayer. *International Journal of Modern Physics C, 26*(01), 1550009. [CrossRef]

[43] Qin, Z., Qin, G., Zuo, X., Xiong, Z., & Hu, M. (2017). Orbitally driven low thermal conductivity of monolayer gallium nitride (GaN) with planar honeycomb structure: a comparative study. *Nanoscale, 9*(12), 4295-4309. [CrossRef]

[44] Van de Walle, C. G., & Neugebauer, J. (2004). First-principles calculations for defects and impurities: Applications to III-nitrides. *Journal of applied physics, 95*(8), 3851-3879. [CrossRef]

[45] Zhang, S. B., & Northrup, J. E. (1991). Chemical potential dependence of defect formation energies in GaAs: Application to Ga self-diffusion. *Physical review letters, 67*(17), 2339. [CrossRef]

[46] Jiang, J., Feng, W., Wen, Y., Yin, L., Wang, H., Feng, X., ... & He, J. (2023). Tuning 2D magnetism in cobalt monoxide nanosheets via in situ nickel-doping. *Advanced Materials, 35*(22), 2301668. [CrossRef]

[47] Li, J., & Liu, H. (2018). Magnetism investigation of GaN monolayer doped with group VIII B transition metals. *Journal of Materials Science, 53*(23), 15986-15994. [CrossRef]

Yi Luo is a lecturer and master's supervisor at the School of Mechanical Engineering, Jiangsu Ocean University, Lianyungang 222005, China. Her research focuses on first-principles calculations of two-dimensional materials. (Email: yiluo9451@outlook.com)

Weiye He is currently pursuing a PhD at the School of Materials Science and Engineering, Northeastern University, Shenyang 110819, China. His research focuses on theoretical calculations of the properties of two-dimensional semiconductor materials. (Email: 13621503175@163.com)

Jilin Xu is a lecturer and master's supervisor at the School of Mechanical Engineering, Jiangsu Ocean University, Lianyungang 222005, China. His research focuses on theoretical and experimental investigations of laser processing and vibration-assisted machining. (Email: xujilin2018@163.com)

Lijie Zuo is an associate professor and master's supervisor at the School of Mechanical Engineering, Jiangsu Ocean University, Lianyungang 222005, China. His research focuses on the design and development of high-strength, high-toughness, heat-resistant aluminum alloys and the investigation of their properties. (Email: zuolijie@126.com)

Feng Shang is a lecturer and master's supervisor at the School of Mechanical Engineering, Jiangsu Ocean University, Lianyungang 222005, China. His research focuses on powder-based near-net-shape forming technologies and corrosion-resistant alloys for marine engineering applications. (Email: shangfeng@jou.edu.cn)

Wen Feng is an associate professor and master's supervisor at the School of Mechanical Engineering, Jiangsu Ocean University, Lianyungang 222005, China. His research focuses on strengthening and toughening metallic materials through grain-boundary engineering, control of second-phase precipitation, and regulation of stacking-fault energy. (Email: wenfeng0327@163.com)

Qianyi Ma is a Postdoc Fellow from the department of chemical engineering at University of Waterloo, Canada. He received his PhD's degree at the University of Waterloo in 2025. His research interests are electrochemical energy storage and conversion, especially for the research of Cathode materials in Li-ion batteries. (Email: q36ma@uwaterloo.ca)